Digitally tunable, wide-band amplitude, phase, and frequency detection for atomic-resolution scanning force microscopy

Z. Khan,[1] C. Leung,[1] B. A. Tahir,[1,2] and B. W. Hoogenboom[1,3,a)]
[1]*London Centre for Nanotechnology, University College London, 17-19 Gordon Street, London WC1H 0AH, United Kingdom*
[2]*Department of Radiotherapy Physics, Weston Park Hospital, Sheffield Teaching Hospitals NHS Trust, Sheffield S10 2SJ, United Kingdom*
[3]*Department of Physics and Astronomy, University College London, Gower Street, London WC1E 6BT, United Kingdom*

(Received 29 April 2010; accepted 7 June 2010; published online 14 July 2010)

Frequency-modulation atomic force microscopy (FM-AFM) relies on an accurate tracking of the resonance frequency of a scanning probe. It is now used in environments ranging from ultrahigh vacuum to aqueous solutions, for slow and for fast imaging, with probes resonating from a few kilohertz up to several megahertz. Here we present a versatile experimental setup that detects amplitude, phase, and frequency of AFM probes for resonance frequencies up to 15 MHz and with >70 kHz maximum bandwidth for amplitude/phase detection. We provide generic parameter settings for variable-bandwidth frequency detection and test these using our setup. The signal-to-noise ratio of the frequency detector is sufficiently high to record atomic-resolution images of mica by FM-AFM in aqueous solution. © *2010 American Institute of Physics.*
[doi:10.1063/1.3458009]

I. INTRODUCTION

Dynamic-mode atomic force microscopy (AFM) enables us to image a wide variety of surfaces at nanoscale resolution. Compared with static- or contact-mode AFM, it has the advantages of minimizing drag forces while scanning and of enabling stable operation in the ranges of both repulsive and attractive forces. The technique is also much less susceptible to drift.[1,2] Dynamic AFM has been operated in various modes, with intermittent-contact or tapping mode being the most straightforward, as it simply relies on detecting the amplitude of the oscillating cantilever as a function of the probe-sample interaction. In spite of some added instrumental complexity, frequency-modulation (FM) AFM has proven to be a more accurate way of controlling (and thereby minimizing) probe-sample forces. Unlike tapping mode, it relies on instantaneous changes in the cantilever oscillation (its resonance frequency), on a purely harmonic oscillation, and it allows a clear separation between elastic and dissipative interactions.[3] It is the method of choice for AFM in ultrahigh vacuum, where atomic resolution has been achieved on many different surfaces.[2] More recently, it has also emerged as a very powerful method in aqueous environment, where it has yielded atomic resolution on mica[4,5] and calcite,[6] and submolecular resolution on a variety of biological samples,[5,7] including channel proteins freely floating in native membranes.[8]

To detect the resonance frequency of a cantilever, the most common method is by a phase-locked loop (PLL), of which various home-built and commercial versions are now available for AFM.[9–19] An alternative method for frequency detection is given by Mitani *et al.*[20] Typically, these frequency detectors are set up for resonance frequencies between some kilohertz up to a few megahertz, which is largely sufficient for conventionally sized cantilevers. However, to gain in signal-to-noise as well as in imaging speed,[21] cantilever dimensions have been reduced to the nanoscale,[22–25] resulting in resonance frequencies up to many tens of megahertz. Megahertz resonance frequencies have also been successfully used for atomic-resolution imaging via higher modes of cantilever oscillation in vacuum.[26–28] This range expands beyond the limits of most frequency detectors in commercially available AFM controllers.

Here we present a frequency detector that mainly consists of radio-frequency (rf) analog components, circumventing speed limitations of standard (low frequency) electronics as well as that of digital implementations of PLLs. It detects a frequency range between 40 kHz and 15 MHz, significantly enhancing the upper detection range compared to most commercial systems. Currently, the upper frequency is only limited by the function generator that creates the reference signals for the PLL. In common with the latest digital implementations of PLLs, the gain parameters of our PLL can be freely adjusted to yield the bandwidth that is most appropriate for the experiment to be carried out.

As for any system that involves nonlinear feedback, however, optimizing the PLL parameters is not trivial. The therefore required knowledge of control theory[29] is not part of the usual skill set of scanning probe microscopists. This has been recognized by recent work on tuning PLLs for an AFM experiment where the PLL reference signal is used to drive the probe oscillation.[30,31] However, in many cases the probe is driven by its own phase-shifted and amplified thermal noise,[2] and the PLL is (only) used to detect the fre-

a)Electronic mail: b.hoogenboom@ucl.ac.uk.

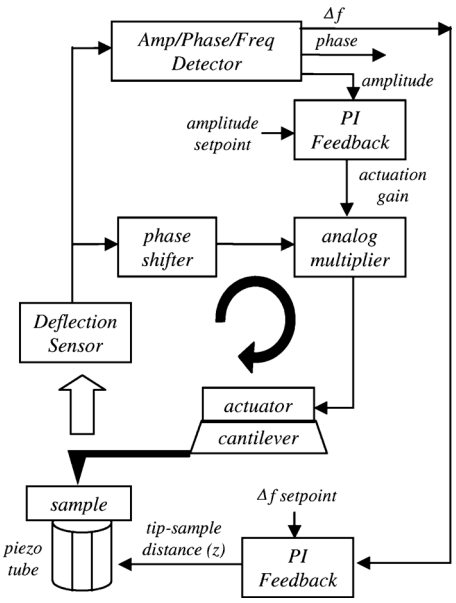

FIG. 1. Block diagram of FM-AFM, displaying the cantilever above the sample, the self-oscillation feedback loop, and the amplitude, phase, and frequency detector. Adapted from Ref. 2.

quency of this so-called self-oscillation (see Fig. 1). For the latter case no generic parameter settings are available in the scanning probe literature. We have derived such settings in physically meaningful units and tested them using our experimental setup.

We describe our setup for FM-AFM, the electronics design, as well as the (theoretical) parameter settings in Sec. II. Next we characterize the frequency range, the modulation bandwidth for phase and thus also amplitude detection, and the step-response for various settings of the PLL in Sec. III. We conclude Sec. III with a demonstration of the use of the PLL for AFM in liquid, by imaging mica in aqueous solution at atomic resolution.

II. INSTRUMENTAL SETUP

A. FM-AFM

Figure 1 shows the block diagram of our AFM. The tip is brought close to the sample, and the vertical deflection of the cantilever is measured by an optical deflection sensor[32,33] and fed into the amplitude, phase, and frequency detector. In standard intermittent-contact/tapping mode, the cantilever is driven (via an actuator) by a sine wave from an actuator with fixed frequency. The detected amplitude or phase is used as the input to the proportional-integral (PI) feedback that governs the tip-sample distance (PI feedback at the bottom of Fig. 1).

In FM-AFM, the deflection signal is phase shifted and amplified before being fed into the cantilever actuator.[2] The phase and gains are adjusted such that a stable self-oscillation is achieved at the resonance frequency of the cantilever. This is equivalent to the so-called Q-control used in air and liquid environment.[34] A digitally controlled analog PI feedback (SRS SIM960, Sunnyvale, CA) adjusts the gain to keep the amplitude of the oscillation at a set value. The tip-sample interaction results in a shift Δf of the resonance frequency of this oscillation. The feedback at the bottom of Fig. 1 then adjusts the tip-sample distance to keep Δf constant.

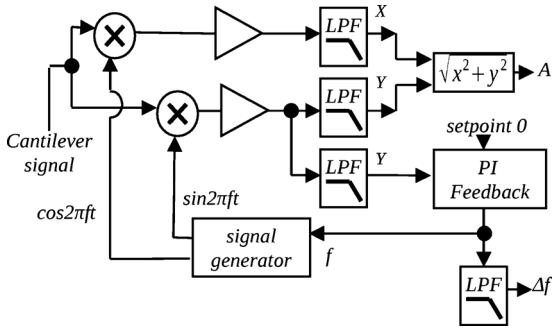

FIG. 2. Block diagram of the electronics for the amplitude, phase, and frequency detector (see text).

In an alternative arrangement for FM-AFM (see, e.g., Ref. 5), the self-oscillation loop can be omitted and the cantilever is driven by a signal with the (varying) reference frequency of the frequency detector. This reduces fluctuations in amplitude, but also implies a lower effective quality factor (relevant in liquid environment).

B. Electronics design

The first stage of our electronics is essentially equivalent to an analog lock-in amplifier, but based on 50 Ω rf components (Mini-Circuits, Brooklyn, NY). The cantilever signal is fed into a transformer (T1-6-X65+, frequency range: 10 kHz–150 MHz), which removes the dc component from the lock-in input and helps to avoid ground loops. The signal is then split by a 50 Ω four-way splitter (PSC-4-6+, 10 kHz–40 MHz), resulting in a signal for the self-oscillatory loop (see Fig. 1), a signal for an oscilloscope, and two signals to be fed into the mixers (SRA-6+, 3 kHz–100 MHz) (see Fig. 2). The references $\cos(2\pi ft)$ and $\sin(2\pi ft)$ for the mixers are provided by a signal generator (Yokogawa FG220/R1, 1 μHz–15 MHz, Tokyo, Japan). The signal generator contains an analog input to modulate the frequency (or phase or amplitude) with a modulation bandwidth of 70 kHz. Standard rf sine generators can be modulated significantly faster, but do not offer the same flexibility of operation. The signal generator is used to modulate the frequency of the reference signals. The signal generator thus acts as a voltage-controlled oscillator (VCO), of which the frequency span can be adjusted. The rf frequencies of the mixer outputs are removed by a 1.9 MHz low-pass filter (LPF, PLP-1.9+, not shown in block diagram), and the remaining low-frequency signals are amplified by a conventional amplification stage.

The dc values of these signals now correspond to the projections of the signal on the X [real, $\cos(2\pi ft)$] and Y [imaginary, $\sin(2\pi ft)$] axes of the complex plane, as in a standard lock-in amplifier. Compared with commercially available lock-ins, however, these outputs are at least an order of magnitude faster. The same applies to the speed at which the reference frequency can be modulated.

For the amplitude (A) measurement, X and Y are fed into a stage with 25 kHz LPFs, rectifiers (AD822), and a vectorial sum amplifier (AD538). The Y signal is also fed into a digi-

tally controlled second order LPF Bessel filter (SRS SIM965, with maximum characteristic frequency $f_s = 500$ kHz). Typically the reference signals are adjusted such that the cantilever oscillation is roughly aligned along the X axis in the imaginary plane. In that case, $Y \approx A\phi$, such that the signal phase can be determined with a variable bandwidth up to a 3 dB cutoff of $f_{s,-3\ \mathrm{dB}} \approx f_s \times 0.7862 \approx 400$ kHz.

In this setup, frequency detection is performed by a PLL. We recall that a PLL consists of a phase detector (here: mixer and amplifier for the Y output), a loop filter (here: Bessel filter and PI feedback—with setpoint zero—SRS SIM960), and a VCO (here: the signal generator).[29] In short, a PLL nullifies its phase input by adjusting its reference frequency (so-called center frequency). A zero phase signal can only be achieved by exactly matching the reference frequency to the frequency of the signal at the PLL input (here: the cantilever signal). The output of the PI feedback (input of the VCO) then provides a measure of the cantilever oscillation frequency.

C. Tuning the frequency detector

The bandwidth of the amplitude and phase detection is directly set by the use of LPFs. The bandwidth and stability of the frequency detection critically depend on the settings of the PI feedback for the PLL. If we neglect the LPF, the PLL is of second order and the open-loop gain can be described by

$$\Delta f(s) = \frac{P}{s}\frac{1+s\tau_i}{s\tau_i}\theta_{\mathrm{error}}(s), \tag{1}$$

where Δf is the detected frequency shift, s is the complex frequency, i.e., $s = \mathrm{i}\omega = \mathrm{i}2\pi f$, and θ_{error} is the input of the phase detector (the phase difference between signal and reference).[29] The PI feedback is defined by P, the proportional gain in Hz/degree, and τ_i, the integration time constant.

In this case, the PLL bandwidth can be determined analytically. The -3 dB cutoff for frequency detection ("modulation bandwidth") is

$$f_{\mathrm{PLL},-3\ \mathrm{dB}} = f_n\sqrt{1+2\zeta^2+\sqrt{(1+2\zeta^2)^2+1}}, \tag{2}$$

where f_n is the natural frequency of the PLL and ζ a dimensionless damping coefficient.[29] Relevant choices for the damping are: $\zeta = 1/\sqrt{2}$ for a Butterworth-like response (resulting in $f_{\mathrm{PLL},-3\ \mathrm{dB}} = f_n \times 2.05817\ldots$); $\zeta = \sqrt{3}/2$ for the minimum-overshoot response of a Bessel filter (resulting in $f_{-3\ \mathrm{dB}} = f_n \times 2.27872\ldots$); and $\zeta = 1$ for critical damping (resulting in $f_{\mathrm{PLL},-3\ \mathrm{dB}} \approx f_n \times 2.48239$).

To achieve frequency detection with a bandwidth of $f_{\mathrm{PLL},-3\ \mathrm{dB}}$ and a damping coefficient ζ, we determine the natural frequency f_n from Eq. (2) and, subsequently[29] set the PI parameters according to

$$P = \frac{\pi\zeta f_n}{90}, \tag{3}$$

$$\tau_i = \frac{\zeta}{\pi f_n}. \tag{4}$$

TABLE I. Theoretical parameter settings for PI feedback and filters to yield 1 kHz modulation bandwidth with a second and fourth order PLLs (see text). For other bandwidths, note that τ_i is inversely proportional, and P and f_s are proportional to $f_{\mathrm{PLL},-3\ \mathrm{dB}}$.

	Second order PLL			
	$\zeta = 1$	$\zeta = \sqrt{3}/2$	$\zeta = 1/\sqrt{2}$	Fourth order PLL
P [Hz/degree]	14.1	13.3	12.0	13.1
τ_i [ms]	0.790	0.628	0.463	0.212
f_s [kHz]	∞ [a]	∞ [a]	∞ [a]	3.76

[a]In practice, optimum fourth-order behavior is obtained using the second-order parameters with $f_s \gtrapprox 5 f_{\mathrm{PLL},-3\ \mathrm{dB}}$.

The situation is more complicated if we also take into account the LPF between the phase detector and the PI feedback, such as the one used to eliminate the sum-frequency component of the mixer outputs. Here we consider a second order LPF, which yields a fourth order PLL and results in a modified open-loop gain of

$$\Delta f(s) = \frac{P}{s}\frac{\omega_s^2}{s^2+2s\omega_s\zeta_s+\omega_s^2}\frac{1+s\tau_i}{s\tau_i}\theta_{\mathrm{error}}(s), \tag{5}$$

where $\omega_s = 2\pi f_s$ and ζ_s are the natural frequency and damping coefficient of the second order filter, respectively. As before, $\zeta = 1/\sqrt{2}$ for a Butterworth filter (with -3 dB cutoff $f_{s,-3\ \mathrm{dB}} = f_s$), and $\zeta_s = \sqrt{3}/2$ for a Bessel filter (with -3 dB cutoff $f_{s,-3\ \mathrm{dB}} \approx f_s \times 0.7862$).

Following the procedure in Ref. 29, we define the transition frequency f_T as the frequency for which the open-loop gain is 1, and estimate $f_{\mathrm{PLL},-3\ \mathrm{dB}} \approx f_T \times 1.33$. The PI feedback and filter settings for a modulation bandwidth of $f_{\mathrm{PLL},-3\ \mathrm{dB}}$ then follow from

$$P = \frac{\pi f_T}{180}, \tag{6}$$

$$\tau_i = \frac{1}{2\pi f_T}, \tag{7}$$

$$f_s = 5 f_T. \tag{8}$$

Table I summarizes the parameters for the various scenarios as discussed above, for $f_{-3\ \mathrm{dB}} = 1$ kHz. The settings for other bandwidths can easily be derived from these values, since τ_i is inversely proportional, and P and f_s are proportional to $f_{\mathrm{PLL},-3\ \mathrm{dB}}$ [see Eqs. (3), (4), and (6)–(8)]. Table I can thus be used to derive parameter settings for any modulation bandwidth and is generic for PLLs with standard PI feedback as a loop filter.

In our setup the bandwidth is currently limited by the modulation input of the signal generator. This input corresponds to a second order Bessel filter with $f_s \approx 90$ kHz [i.e., a LPF with 3 dB cutoff at 70 kHz). As a consequence, if we adhere to the settings from Eqs. (6)–(8)] for the fourth order PLL, the maximum theoretical bandwidth for frequency detection is $90/3.76 \approx 25$ kHz. In that case, the external LPF is bypassed or set to a value $\gg 90$ kHz, and the loop filter is provided by the PI feedback and the modulation input of the signal generator.

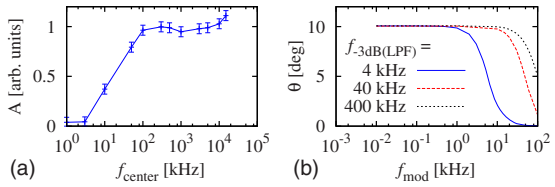

FIG. 3. (Color online) (a) Amplitude detection as a function of the center frequency of the carrier oscillation. (b) The detected phase modulation for an input signal that is (±10°) phase-modulated with a modulation frequency f_{mod}.

III. CHARACTERIZATION AND DISCUSSION

A. Amplitude and phase detection

Our experimental setup can detect oscillations over a frequency range of about 40 kHz–15 MHz. To demonstrate this, we fed an oscillatory test signal to the input of the electronics ("cantilever signal") and varied its frequency. The center frequency was continuously adjusted to match the signal frequency. Thus the amplitude A of the test signal was measured over the full frequency range [see Fig. 3(a)]. The lower-frequency cutoff is caused by a high-pass filter at the input (not shown in diagram), the higher-frequency limit is set by the maximum frequency of the signal generator.

The effect of the adjustable LPFs (see Fig. 2) can be shown by providing the electronics with a ±10° phase-modulated signal with carrier frequency 1 MHz and modulation frequency f_{mod}, and monitoring the Y output as a function of f_{mod}. Here, we used the cosine channel of the signal generator as an input signal, phase-modulated via the external analog modulation input of the signal generator. This was done for different settings of the natural frequency f_s of the second order Bessel filter: f_s=5, 50, and 500 kHz, implying 3 dB cutoffs of the Bessel filter of $f_{s,-3\ dB} \approx 4$ kHz, 40 Hz, and 400 kHz, respectively. As can be read of Fig. 3(b), the measured cutoffs for the phase detector are 4, 34, and 68 kHz for these settings. For low frequencies (up to 30–40 kHz), the setting of the LPFs determines the modulation bandwidth of the phase detector. For higher frequencies, the modulation bandwidth is mainly limited by the modulation bandwidth of the signal generator that provides the input signal (≈70 kHz, see end of Sec. II C): that is to say that, though phase detection is much faster, the test signal could not be modulated faster than 70 kHz. The limit for phase detection will thus be significantly faster, and is expected to be only limited by the $f_{s,-3\ dB}$ of the Bessel filter. The setup is therefore a valuable alternative to more complicated schemes for high-speed phase detection.[35]

B. Frequency detection

To characterize the frequency detector, we have studied its response to steps in the carrier frequency at the entrance of the detector, for different PLL settings based on the parameters displayed in Table I. $f_{PLL,-3\ dB}$=1.2 kHz is chosen [Figs. 4(a) and 4(b)] to facilitate comparison to a commercial frequency detector (Nanosurf EasyPLL, Liestal, Switzerland) [Fig. 4(d)]. A 100 mV_{rms} 100 kHz signal was provided to the input of the frequency detector (source: reference channel of an SRS830 lock-in amplifier), and changed in steps of 10 Hz.

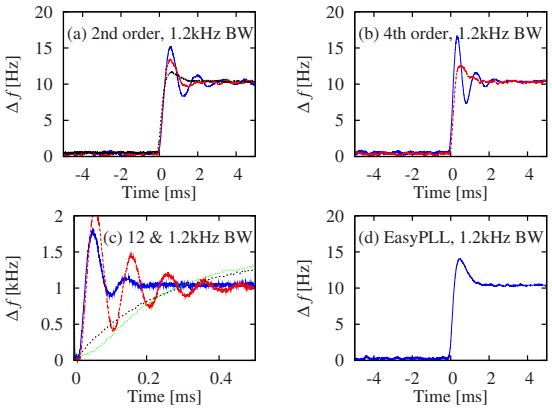

FIG. 4. (Color online) Frequency step-response. (a) Second order PLL with $f_{PLL,-3\ dB}$=1.2 kHz, for ζ=0.3 (solid line), ζ=0.5 (dashed), $\zeta=\sqrt{3}/2$ (dotted). (b) Fourth order PLL with theoretical settings (solid) and with second-order settings for $\zeta=\sqrt{3}/2$ and $f_s=5f_{PLL,-3\ dB}$ (dashed). (c) Second-order settings for $\zeta=\sqrt{3}/2$ and $f_{PLL,-3\ dB}$=12 kHz, with $f_s=\infty$ (solid) and $f_s=5f_{PLL,-3\ dB}$ (dashed), compared to the equivalent $f_{PLL,-3\ dB}$=1.2 kHz settings (short dash and dotted). (d) Step-response of a commercial frequency detector (Nanosurf EasyPLL).

For the second order PLL, the step-response shows undesirable oscillatory behavior for low damping (ζ=0.3–0.5), which disappears for the ideal damping coefficients from Table I. The behavior for $\zeta=1/\sqrt{2}$ and ζ=1 (not shown) hardly deviates from that of the $\zeta=\sqrt{3}/2$ [Fig. 4(a)]. The parameters from the phenomenological procedure for the fourth order PLL (Table I fourth order and Ref. 29) lead to oscillatory step-response, as could be anticipated from direct comparison of the fourth and second order parameters. In practice, we found that the second order parameters yield near-ideal step-response for the fourth order PLL, provided that f_s for the LPF is set at $f_s \gtrapprox 5f_{PLL,-3\ dB}$ [Fig. 4(b)]. This still maintains a sufficient phase margin for the PLL to avoid undesirable overshoot and instabilities.

To demonstrate the high-frequency and high-speed characteristics of the frequency detector, we also provided the detector with a 100 mV_{rms} 10 MHz input signal (source: BK Precision rf signal generator 2005B, Yorba Linda, CA) and studied the response following a sudden additional offset on the output of the PI feedback (see Fig. 2) at t=0 ms [Fig. 4(c)]. The phase drop at the modulation input of the signal generator (see end of Sec. II C) becomes noticeable via the increased oscillatory behavior in Δf compared to the lower-bandwidth settings. With $f_{-3\ dB}$=12 kHz, the second order and fourth order PLL responses both show a rise time (10%–90% of step) τ_{rise}=13 μs as expected for $f_{-3\ dB}$=12 kHz, sufficiently fast for AFM feedback with scan times $\lesssim$1 s per image of ~100×100 pixels.

C. Imaging at atomic resolution

Finally, to demonstrate the performance of the frequency detector for actual AFM operation, we used a Veeco Multimode scan system with an A-scanner and a home-built optical head.[32,33] The output of the frequency detector was connected to the deflection input of a Veeco Nanoscope III controller. As a benchmark experiment,[4,5] we imaged the surface of cleaved muscovite mica in aqueous solution

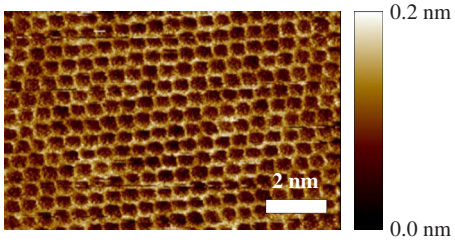

FIG. 5. (Color online) FM-AFM topograph of the surface of cleaved mica in aqueous solution. The Nanosensors PPP-NCH cantilever (spring constant 42 N/m) was kept at a constant amplitude of 0.6 nm and at a constant frequency shift of ~100 Hz with respect to its resonance away from the surface (158 kHz). The tip velocity was 61 nm/s.

(150 mM KCl, 20 mM Tris-HCl, pH 7.0). The result is shown in Fig. 5. The image was flattened and the scaling of the *x* and *y* axes was adjusted to correct for nonlinearity of the *xy* piezos, but otherwise represents the raw, unfiltered data. The honeycomb structure of the atomic lattice is clearly visible, as well a height variations between different unit cells, suggesting atomic-scale defects.

IV. CONCLUSION

We have developed a digitally tunable amplitude, phase, and frequency detector for high-resolution AFM. Based on rf components, it has an operating range between 40 kHz and 15 MHz, which can be extended to 100 MHz by replacing the generator of the reference signal (limited to a maximum of 15 MHz in our setup). Amplitude and phase modulation can theoretically be measured in a modulation bandwidth of up to 400 kHz with the current setup, with experimentally demonstrated modulation >70 kHz (70 kHz being the maximum speed at which the test signal was modulated). In our setup, frequency detection was performed with modulation bandwidths up to about 12 kHz.

We have derived the generic parameter settings for detection of cantilever resonance frequencies with various bandwidths, and tested these using our experimental setup. We expect this type of setup to be a valuable alternative for AFM with megahertz-frequency cantilevers and the parameters settings to be a valuable resource for atomic force microscopists using FM in home-built and commercial instruments.

ACKNOWLEDGMENTS

We gratefully acknowledge financial support from the UK Engineering and Physical Sciences Research Council (EPSRC) and the UK Biotechnology and Biological Science Research Council (BBSRC, BB/G011729/1). We thank S. Kawai and H. J. Hug for useful discussions.

[1] R. García and R. Pérez, Surf. Sci. Rep. **47**, 197 (2002).
[2] F. J. Giessibl, Rev. Mod. Phys. **75**, 949 (2003).
[3] T. R. Albrecht, P. Grütter, D. Horne, and D. Rugar, J. Appl. Phys. **69**, 668 (1991).
[4] T. Fukuma, K. Kobayashi, K. Matsushige, and H. Yamada, Appl. Phys. Lett. **87**, 034101 (2005).
[5] B. W. Hoogenboom, H. J. Hug, Y. Pellmont, S. Martin, P. L. T. M. Frederix, D. Fotiadis, and A. Engel, Appl. Phys. Lett. **88**, 193109 (2006).
[6] S. Rode, N. Oyabu, K. Kobayashi, H. Yamada, and A. Kühnle, Langmuir **25**, 2850 (2009).
[7] H. Yamada, K. Kobayashi, T. Fukuma, Y. Hirata, T. Kajita, and K. Matsushige, Appl. Phys. Express **2**, 095007 (2009).
[8] B. W. Hoogenboom, K. Suda, A. Engel, and D. Fotiadis, J. Mol. Biol. **370**, 246 (2007).
[9] C. Loppacher, M. Bammerlin, F. Battiston, M. Guggisberg, D. Müller, H. R. Hidber, R. Lüthi, E. Meyer, and H. J. Güntherodt, Appl. Phys. A **66**, S215 (1998).
[10] K. Kobayashi, H. Yamada, H. Itoh, T. Horiuchi, and K. Matsushige, Rev. Sci. Instrum. **72**, 4383 (2001).
[11] S. Kawai, D. Kobayashi, S.-I. Kitamura, S. Meguro, and H. Kawakatsu, Rev. Sci. Instrum. **76**, 083703 (2005).
[12] H.-P. Rust, M. Heyde, and H.-J. Freund, Rev. Sci. Instrum. **77**, 043710 (2006).
[13] Asylum Research, Santa Barbara, CA, www.asylumresearch.com.
[14] JPK Instruments, Berlin, Germany, www.jpk.com.
[15] Nanonis/SPECS Zurich, Zurich, Switzerland, www.specs-zurich.com.
[16] Nanoscan, Duebendorf, Switzerland, www.nanoscan.ch.
[17] Nanosurf, Liestal, Switzerland, www.nanosurf.ch.
[18] Omicron Nanotechnology, Taunusstein, Germany, www.omicron.de.
[19] RHK Technology, Troy, MI, www.rhk-tech.com.
[20] Y. Mitani, M. Kubo, K.-I. Muramoto, and T. Fukuma, Rev. Sci. Instrum. **80**, 083705 (2009).
[21] T. Ando, T. Uchihashi, and T. Fukuma, Prog. Surf. Sci. **83**, 337 (2008).
[22] D. A. Walters, J. P. Cleveland, N. H. Thomson, P. K. Hansma, M. A. Wendman, G. Gurley, and V. Elings, Rev. Sci. Instrum. **67**, 3583 (1996).
[23] H. Kawakatsu, D. Saya, A. Kato, K. Fukushima, H. Toshiyoshi, and H. Fujita, Rev. Sci. Instrum. **73**, 1188 (2002).
[24] J. L. Yang, M. Despont, U. Drechsler, B. W. Hoogenboom, P. L. T. M. Frederix, S. Martin, A. Engel, P. Vettiger, and H. J. Hug, Appl. Phys. Lett. **86**, 134101 (2005).
[25] M. Li, H. X. Tang, and M. L. Roukes, Nat. Nanotechnol. **2**, 114 (2007).
[26] S. Kawai and H. Kawakatsu, Appl. Phys. Lett. **88**, 133103 (2006).
[27] S. Kawai and H. Kawakatsu, Appl. Phys. Lett. **89**, 013108 (2006).
[28] S. Kawai and H. Kawakatsu, Phys. Rev. B **79**, 115440 (2009).
[29] R. E. Best, *Phase-Locked Loops: Design, Simulation, and Applications*, 6th ed. (McGraw-Hill, New York, 2007).
[30] A. E. Gildemeister, T. Ihn, C. Barengo, P. Studerus, and K. Ensslin, Rev. Sci. Instrum. **78**, 013704 (2007).
[31] J. I. Kilpatrick, A. Gannepalli, J. P. Cleveland, and S. P. Jarvis, Rev. Sci. Instrum. **80**, 023701 (2009).
[32] B. W. Hoogenboom, P. L. T. M. Frederix, J. L. Yang, S. Martin, Y. Pellmont, M. Steinacher, S. Zäch, E. Langenbach, H.-J. Heimbeck, A. Engel, and H. J. Hug, Appl. Phys. Lett. **86**, 074101 (2005).
[33] B. W. Hoogenboom, P. L. T. M. Frederix, D. Fotiadis, H. J. Hug, and A. Engel, Nanotechnology **19**, 384019 (2008).
[34] J. Tamayo, A. D. L. Humphris, and M. J. Miles, Appl. Phys. Lett. **77**, 582 (2000).
[35] T. Uchihashi, T. Ando, and H. Yamashita, Appl. Phys. Lett. **89**, 213112 (2006).